Comparative Study of the Uniaxial Cyclic Behaviour of Carbide-Bearing and Carbide-Free Bainitic Steels

Ricardo Branco [1],* [ID], Filippo Berto [2], Fucheng Zhang [3,4], Xiaoyan Long [3] and José Domingos Costa [1]

[1] CEMMPRE, Department of Mechanical Engineering, University of Coimbra, Rua Luís Reis Santos, 3030-788 Coimbra, Portugal; jose.domingos@dem.uc.pt

[2] Department of Mechanical and Industrial Engineering, Norwegian University of Science and Technology (NTNU), Richard Birkelands vei 2b, 7491 Trondheim, Norway; filippo.berto@ntnu.no

[3] State Key Laboratory of Metastable Materials Science and Technology, Yanshan University, Qinhuangdao 066004, China; zfc@ysu.edu.cn (F.Z.); longxiaoyanlxy@163.com (X.L.)

[4] National Engineering Research Center for Equipment and Technology of Cold Strip Rolling, Yanshan University, Qinhuangdao 066004, China

* Correspondence: ricardo.branco@dem.uc.pt; Tel.: +351-239-790-700

Abstract: Bainitic steels play an important role in the modern automotive and rail industries because of their balanced properties. Understanding the relationship between the bainitic microstructure features and the fatigue performance is a fundamental ingredient in developing safer and durable products. However, so far this relationship is not sufficiently clear. Therefore, there is the need to strengthen the knowledge within this field. The present paper aims at comparing the uniaxial cyclic behaviour of carbide-bearing and carbide-free bainitic steels. To meet this goal, fully-reversed strain-controlled tests at various strain amplitudes were performed. After the final failure, fracture surfaces were observed by transmission electron microscopy to relate the bainitic morphology to the fatigue performance. The main findings of this work show that the carbide-free lower bainite has superior fatigue performance compared to the carbide-bearing lower bainite. This is explained by the presence of stable carbides and thick bainite ferrite plates.

1. Introduction

Bainitic steels play an important role in the modern automotive and rail industries because of their balanced properties in terms of strength, fatigue and fracture characteristics, wear, elongation, machinability, and production costs [1–3]. In this context, understanding the relationship between the bainitic morphology and the mechanical performance of the produced steels is pivotal to meet these requirements and, ultimately, to develop safer and more durable products.

Mechanical performance is directly related to the bainitic morphology and the chemical composition. In the above-mentioned industries, critical components are usually subjected to time-varying loading histories and therefore, superior cyclic mechanical properties are of major engineering significance. According to Georgiyev et al. [4], the highest performance with respect to crack resistance in medium-carbon steels of similar strength is obtained from carbide-free lower bainite microstructures. The main outcome of a recent study published by Long et al. [5] also attests to the improved performance of the carbide-free lower bainitic steels when compared with carbide-bearing lower bainitic steels in a low-cycle fatigue regime.

Nevertheless, systematic studies dealing with fatigue behaviour of carbide-free and carbide-bearing lower bainitic steels are quite scarce [6,7]. Therefore, there is the need to strengthen the research in this

field. From an engineering point of view, as is well-known, fatigue design is usually carried out using stress-based, strain-based, or energy-based relationships [8–10]. In the modern fatigue life prediction models, cyclic plasticity plays a major role and is considered to be the main cause of damage [11,12]. An accurate knowledge of cyclic plastic behaviour is a fundamental ingredient to obtain accurate lifetime predictions, as well as to develop feasible elastic-plastic numerical models [13,14].

The present paper aims at comparing the uniaxial cyclic behaviour of carbide-free and carbide-bearing bainitic steels under fully-reversed strain-controlled conditions. In this ambit, low-cycle fatigue tests at room temperature in standard cylindrical specimens will be performed at various strain amplitudes. Then, the cyclic stress-strain response, the shapes of the hysteresis loops, the fatigue-strength and fatigue-ductility properties, and the plastic strain energy densities of both bainitic steels will be assessed and evaluated. Moreover, before fatigue testing, the microstructures will be analysed by scanning electron microscopy (SEM) and transmission electron microscopy (TEM). After the total failure of the specimens, fracture morphologies will be observed by SEM to relate the phase effects to the cyclic behaviour.

2. Experimental Procedure

Low-cycle fatigue tests, summarised in Table 1, were performed in a 100 kN MTS servo-hydraulic testing machine (MTS, Eden Prairie, MN, USA) under fully-reversed strain-controlled conditions, for strain amplitudes between 0.6% and 1.0%. This was done using sinusoidal waveforms and a constant strain rate of 6×10^{-3} s^{-1}. Each individual test was initiated in tension, and failure was defined as a 25% load drop relative to the maximum load. Hysteresis loops were collected from a uniaxial extensometer. The samples, with a gauge length of 10 mm and a gauge diameter of 5 mm, were fabricated from two bainitic steels [5], termed here carbide-bearing lower bainite and carbide-free lower bainite, whose chemical compositions and mechanical properties are listed in Tables 2 and 3, respectively. Both chemical compositions are virtually the same, except for the content of Si and Al. In the former steel, those elements were alloyed to introduce carbide-free bainite, while in the latter, the elements were not alloyed to introduce carbide-bearing bainite. The contents of S, P, and N are far below 0.01% which means that their effects on the steel performance can be neglected [5]. The steels were synthesised via vacuum smelting and forging, with a forging ratio equal to 6.

Microstructures were observed using a Hitachi H-800 TEM (Hitachi, Tokyo, Japan) operated at 200 kV and a SU-5000 Hitachi thermal-emission SEM (Hitachi, Tokyo, Japan). Before examination, the samples were thinned to perforation on a TenuPol-5 twinjet unit with an electrolyte composed of 7% perchloric and 93% glacial acetic acids. Electropolishing was performed at a temperature of 25 °C and a voltage of 29 V. After the fatigue tests, fracture surfaces were observed by the TEM to characterise the surface morphologies and to identify the main fatigue damage mechanisms.

Table 1. Low-cycle fatigue test program.

Specimen Reference	Total Strain Amplitude, $\Delta\varepsilon/2$ (%)	Elastic Strain Amplitude, $\Delta\varepsilon_e/2$ (%)	Plastic Strain Amplitude, $\Delta\varepsilon_p/2$ (%)	Stress Amplitude, $\Delta\sigma/2$ (MPa)	Plastic strain Energy Density, ΔW_P (MJ/m^3)	Number of Cycles to Failure, N_f
Carbide-bearing lower bainite						
CB-0.6	0.5985	0.4724	0.1261	929.29	3.962	3572
CB-0.7	0.6980	0.4837	0.2143	951.42	6.896	2357
CB-0.8	0.7980	0.4963	0.3017	976.17	9.961	1069
CB-1.0	0.9990	0.5287	0.4703	1040.01	16.541	514
Carbide-free lower bainite						
CF-0.6	0.5995	0.5440	0.0555	1070.00	2.010	6305
CF-0.7	0.6990	0.5906	0.1084	1162.43	4.259	4144
CF-0.8	0.7965	0.6249	0.1716	1229.76	7.138	2003
CF-1.0	0.9950	0.6664	0.3285	1311.62	14.573	783

Table 2. Chemical composition in weight percentage.

Material	C	Si	Mn	Cr	Ni	Mo	Al	S	P	N
Carbide-free lower bainite	0.34	1.48	1.52	1.15	0.93	0.4	0.71	0.003	0.006	0.002
Carbide-bearing lower bainite	0.34	0.01	1.61	1.24	0.96	0.45	0.04	0.002	0.005	0.003

Table 3. Main mechanical properties.

Property	Carbide-Bearing Lower Bainite	Carbide-Free Lower Bainite
Yield strength, σ_{YS} (MPa)	1033	1080
Tensile strength, σ_{UTS} (MPa)	1390	1498
Young's modulus, E (GPa)	198.3	197.4
Total elongation, δ_t (%)	12.5	16.0
HRC	43.6	46.0

3. Results and Discussion

3.1. Microstructure

The microstructures of both carbide-bearing and carbide-free lower bainitic steels that were observed via the SEM and TEM microscopes, are exhibited in Figure 1a–d, respectively. As can be seen in Figure 1a–c, the former is mainly formed by bainitic ferrite (BF) and carbides, with a volume fraction of 5.4%, and was distributed within the bainitic ferrite or between the bainitic ferrite along a certain direction. Whereas, the latter is essentially formed by bainitic ferrite (BF) and retained austenite (RA) of varying sizes, with a volume fraction of 9.9%, and alternating between small sizes (RA1) and large sizes (RA2).

The carbide-bearing lower bainite, when compared with the carbide-free lower bainite, contains thicker bainitic ferrite plates (314 ± 34 nm compared to 133 ± 18 nm) and lower dislocation densities (3.3×10^{15} m^{-2} compared to 4.6×10^{15} m^{-2}). This can be explained by the addition of Si and Al elements in the carbide-free lower bainite, which results in a smaller C-diffusion; inhibition of the precipitation of carbides; and higher distribution of carbon atoms in the retained austenite. Moreover, Al can also increase both the transformation driving force and the nucleation density, giving rise to finer bainitic ferrite plates.

(a)

(b)

Figure 1. *Cont.*

(c)

(d)
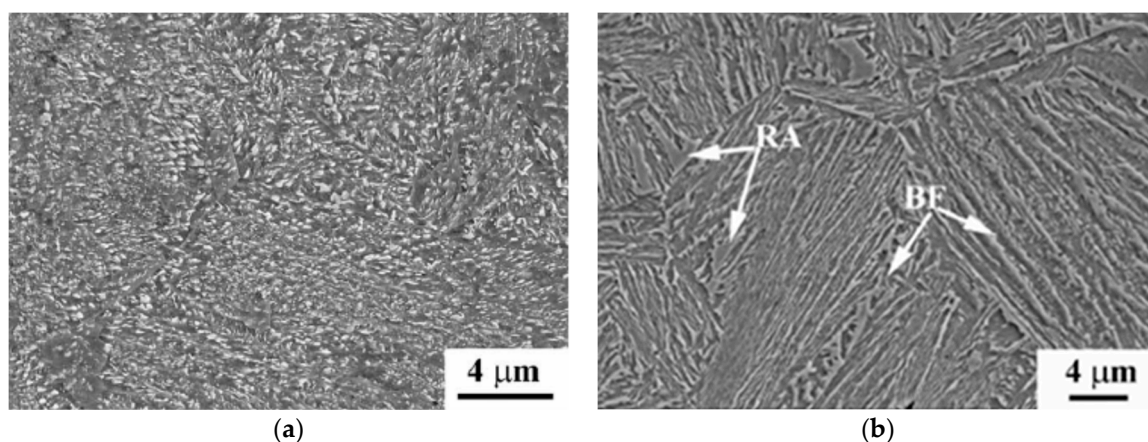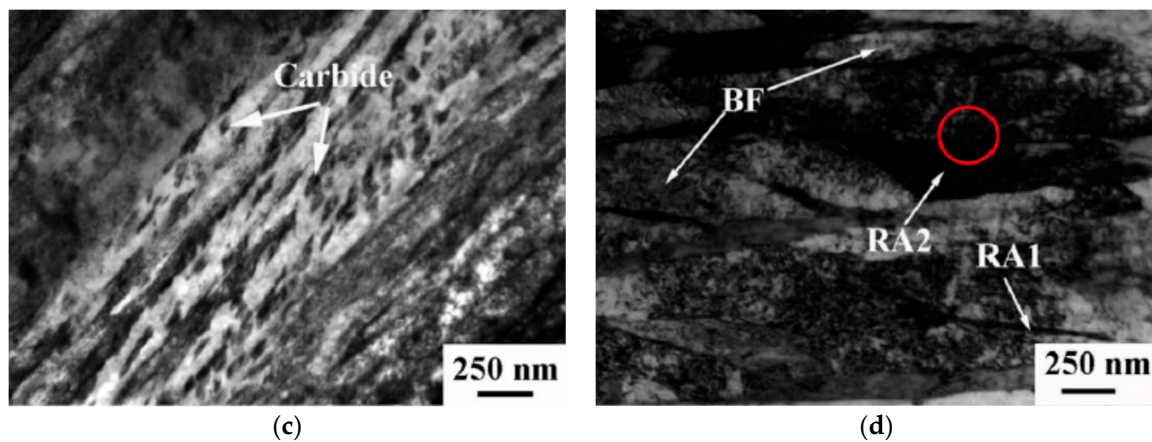
Figure 1. SEM and TEM micrographs [5]: (**a**,**c**) refer to the carbide-bearing lower bainite; (**b**,**d**) refer to the carbide-free lower bainite (RA: Retained austenite; BF: Bainitic ferrite). Reproduced from [5], with permission from publisher Elsevier, 2018.

3.2. Cyclic Stress-Strain Deformation Behaviour

Figure 2 plots the peak stress against the normalised fatigue life (N/N_f) for the carbide-bearing and the carbide-free bainitic steels at different strain amplitudes, under fully-reversed strain-controlled conditions. Both steels, irrespective of the strain amplitude, undergo an initial cyclic hardening with growing intensity in the early cycles, followed by a progressive reduction of peak stress, which is more pronounced for the carbide-bearing bainite. In the second stage, peak stress variations tend to be tenuous, and the material response is close to a saturated state, particularly for the lower strain amplitudes. After this period, in the final stage, the peak stress drops more steeply, leading to total failure.
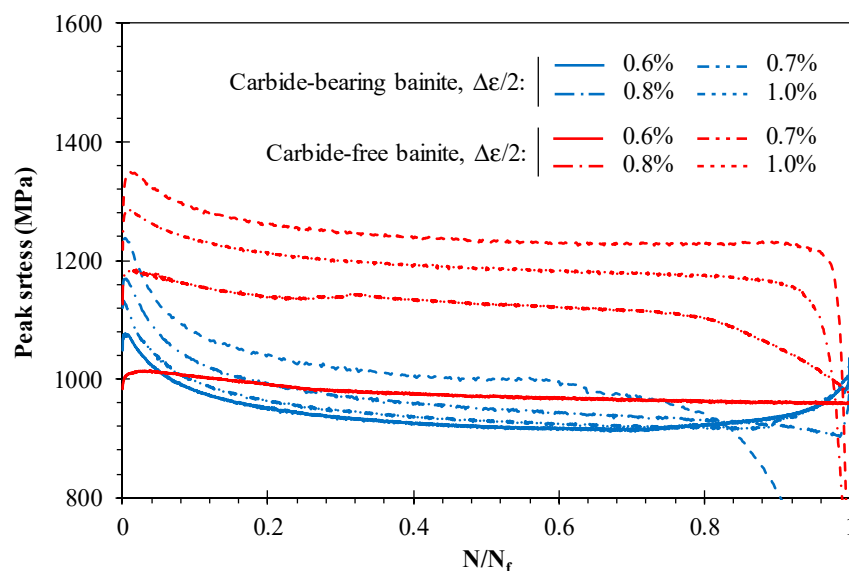
Figure 2. Variation of peak stress with the normalised fatigue life for both carbide-bearing and carbide-free bainitic steels at different strain amplitudes under fully-reversed strain-controlled conditions.

The maximum stress occurs in the early cycles of the tests. The life ratios of these values, designated here by N_p/N_f, are represented in Figure 3a for the tested steels. As can be seen in the figure, although some scatter is observed, there is a clear trend for each case. The maximum stress amplitudes are attained faster for the carbide-bearing lower bainite than for the carbide-free lower

bainite, and the N_p/N_f values are, on average, equal to 0.33% (see the dashed line) and 0.98% (see the dash-dotted line) of the life ratio, respectively.
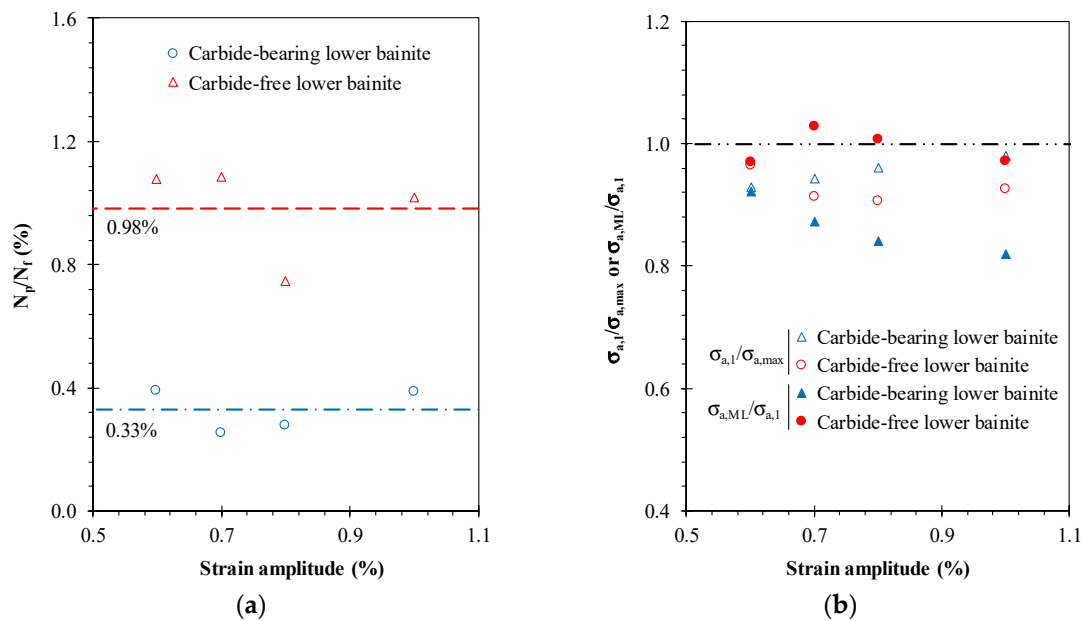
Figure 3. Variation of the: (**a**) N_p/N_f ratio with the strain amplitude; (**b**) $\sigma_{a,1}/\sigma_{a,max}$ and the $\sigma_{a,ML}/\sigma_{a,1}$ ratios with the strain amplitude.

Figure 3b shows, for various strain amplitude levels, the relation between the stress amplitude of the first cycle ($\sigma_{a,1}$) and the maximum stress amplitude ($\sigma_{a,max}$). Both steels have similar relations ($\sigma_{a,1}/\sigma_{a,max}$) slightly below the unity (i.e., 0.93 for the carbide-bearing lower bainite and 0.97 for the carbide-free lower bainite), which denotes cyclic hardening behaviour. As far as what can be inferred from the figure, the above-mentioned relations reach minimum values: (i) at the lowest strain amplitudes for the carbide-bearing lower bainite; and (ii) at intermediate strain amplitudes for the carbide-free lower bainite. With regard to the relations between the stress amplitude of the mid-life cycle ($\sigma_{a,ML}$) and the stress amplitude of the first cycle ($\sigma_{a,1}$), as displayed in Figure 3b, both steels behave differently, i.e., the carbide-bearing bainitic steel exhibits a cyclic softening behaviour with $\sigma_{a,ML}/\sigma_{a,1}$ becoming increasingly lower as the strain amplitude increases, while the other shows a mixed cyclic hardening-softening response that is not particularly intense, with $\sigma_{a,ML}/\sigma_{a,1}$ values quite close to 1.

The study of the cyclic stress-strain response for both tested materials, was performed on the basis of the data being collected for the mid-life cycle [15–17]. Total plastic and elastic strain amplitudes, stress amplitudes, and plastic strain energy densities of the selected hysteresis loops are listed in Table 1. Figure 4a plots the mid-life stress-strain circuits of the carbide-bearing and carbide-free bainitic steels in relative coordinates, with the lower tips tied together at different strain amplitudes. When first looking, it can be concluded that the upper branches are not perfectly coincident, and that we are therefore in the presence of non-Masing type materials. A more in-depth analysis for the carbide-bearing bainitic steel is provided in Figure 4b, which compares perfect Masing-type circuits (dashed lines) with those that were obtained in the experiments (full lines) in relative coordinates, with the upper branches overlapped. Not surprisingly, it is possible to distinguish a reduction of the linear region where, the higher the strain amplitudes, the bigger the differences. The comparison of the mid-life circuits shows that the areas—or in other words, the plastic strain energy densities—are larger for the carbide-bearing lower bainite than for the carbide-free lower bainite (see Table 1) at similar strain amplitude levels.
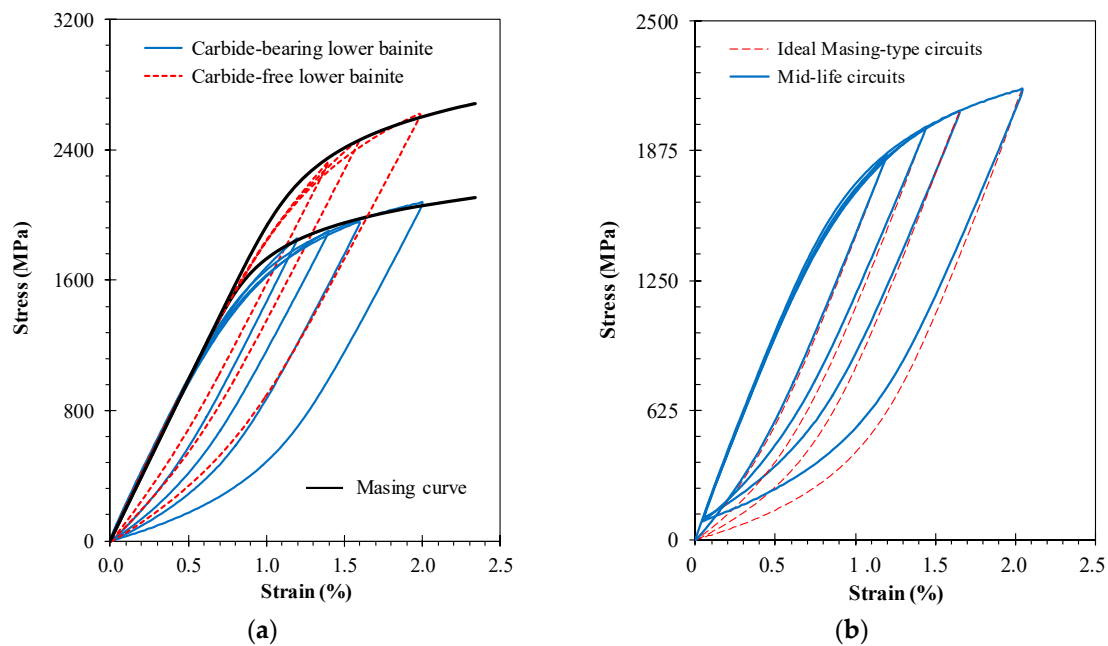
Figure 4. Mid-life circuits at different strain amplitudes with: (**a**) lower tips tied together for the carbide-bearing and carbide-free bainitic steels; (**b**) upper branches overlapped and ideal Masing-type circuits for the carbide-bearing bainitic steel.

The cyclic stress-strain curves, obtained from the mid-life hysteresis circuits, can be seen in Figure 5a. The constants *k′* and *n′* of Equation (1), which respectively represent the cyclic hardening coefficient and the cyclic hardening exponent, were determined using the least square method, and are listed in Table 4. Monotonic stress-strain curves are also plotted for comparison purposes. Both steels behave differently. The carbide-free lower bainite exhibits a strain-hardening response in the entire range, as the experimental cyclic data are above the monotonic curve. On the contrary, the carbide-bearing lower bainite is characterized by a strain-softening behaviour. The degree of strain-hardening (DH) and the degree of strain-softening (DS) are presented in Figure 5b. These variables were accounted for from two different approaches: the first was given by the difference between the stress amplitude of the first and the mid-life circuits (circles and rectangles); and the second was given by the difference between the cyclic and the monotonic curves (dashed lines). The insights drawn from the two approaches are similar: DS increases with the strain amplitude for the carbide-bearing lower bainite and DH decreases with the strain amplitude for the carbide-free lower bainite. Furthermore, the experimental results are close to those collected from the fitted cyclic curves.

$$\frac{\Delta \varepsilon}{2} = \frac{\Delta \sigma}{2E} + \left(\frac{\Delta \sigma}{2k\prime} \right)^{1/n\prime} \tag{1}$$

Figure 6 displays the stress amplitude against the plastic strain amplitude for both of the bainitic steels. These two variables (see the dash-dotted lines) can be related by a power law. Figure 6 also displays the relationship between the stress amplitude and the elastic strain amplitude, which is defined on the basis of the unloading moduli obtained in the experimental tests (see the dashed lines). Similarly, these two variables can also be related via a power law. The *k″* and *n″* constants were determined using the least square method and are summarised in Table 4. The variations of the unloading moduli with the elastic strain amplitude (which are evident when compared with the solid lines—both overlapped—that were obtained from the values of the Young's moduli, given in Table 3) indicate a non-linear behavior, not only in the plastic regime but also in the elastic regime.
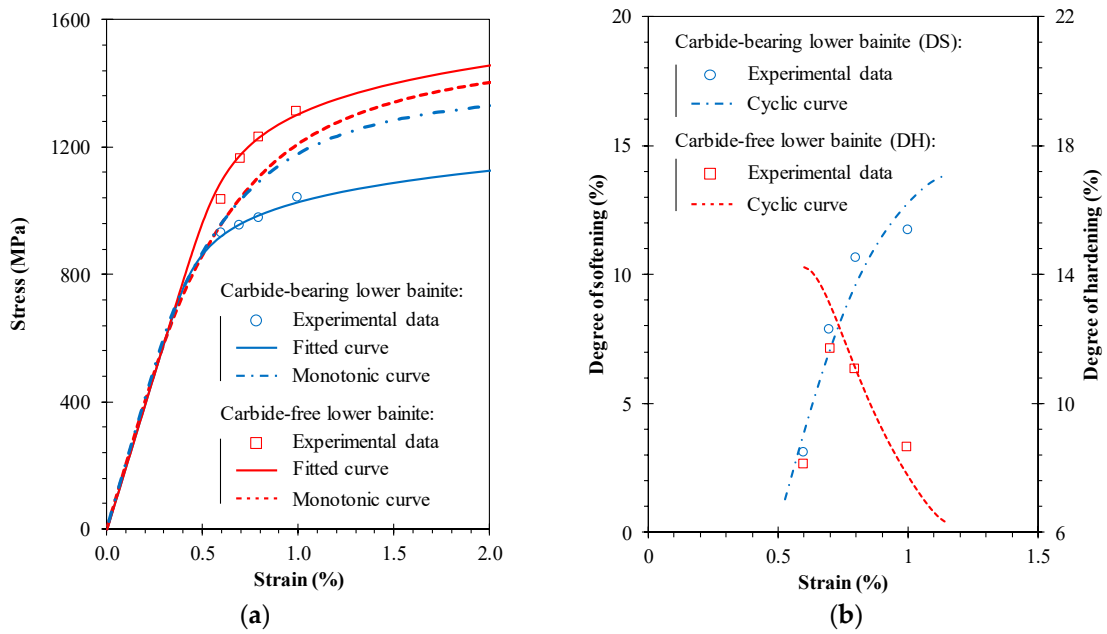
Figure 5. (**a**) Cyclic stress-strain curve; (**b**) variation of the degree of softening and the degree of hardening for the carbide-bearing and carbide-free bainitic steels.

Table 4. Summary of the cyclic mechanical properties.

Material	k' (MPa)	n'	k'' (MPa)	n''
Carbide-bearing lower bainite	1093.60	0.08374	19,823.03	0.57854
Carbide-free lower bainite	1427.49	0.08421	42,027.73	0.70602
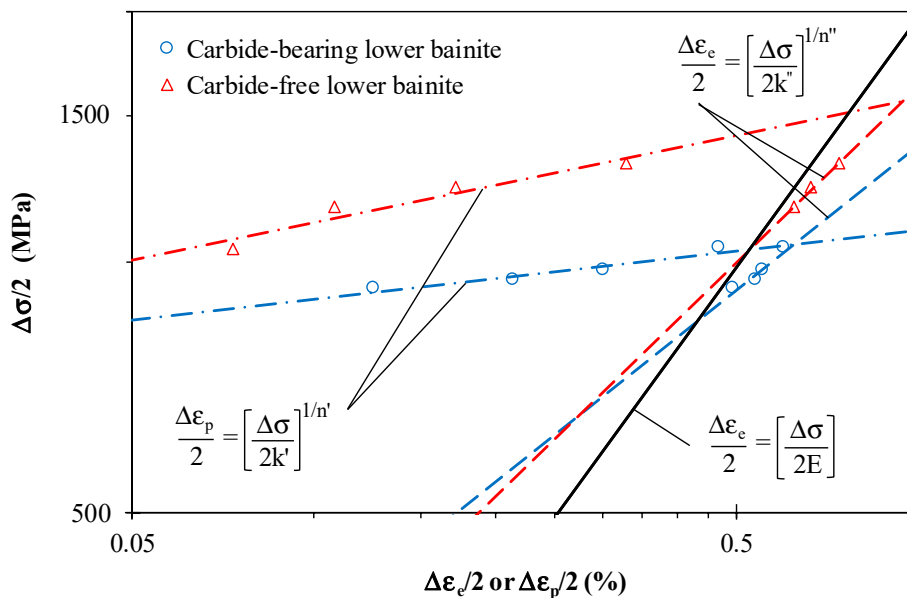
Figure 6. Stress amplitude versus elastic strain amplitudes on the basis of both of the unloading Young's moduli that were evaluated in the tests (dashed lines) and the Young's modulus that was determined from the monotonic tensile test (solid lines).

The stress-life relations, expressed in terms of the number of reversals to failure versus stress amplitude of the mid-life circuits, can be written in the following form:

$$\frac{\Delta\sigma}{2} = \sigma_f' \left(2N_f\right)^{b}$$

(2)

where σ_f' is the fatigue strength coefficient, and b is the fatigue strength exponent. The constants, determined via the least square method, are reported in Table 5. In both cases, but particularly for the carbide-bearing lower bainite, a significant correlation between the experiments and the proposed functions was obtained [5]. As already noted by Long et al. [5], the carbide-free bainite can deal with higher stress amplitudes for a similar number of cycles, particularly for lower fatigue lives. As the fatigue life increases, the differences tend to be attenuated.

The total strain amplitude, defined as the sum of the elastic and plastic parts, can be related to the fatigue life from the following equation:

$$\frac{\Delta\varepsilon}{2} = \frac{\sigma_f'}{E} \left(2N_f\right)^{b} + \varepsilon_f' \left(2N_f\right)^{c}$$

(3)

where σ_f' is the fatigue strength coefficient, b is the fatigue strength exponent, ε_f' is the fatigue ductility coefficient, and c is the fatigue ductility exponent. Figure 7 presents the strain-life relations of the carbide-bearing and the carbide-free steels that were obtained from the experiments. The constants, fitted using the least square method, are reported in Table 5, where the experimental data that was collected in the tests were omitted for the sake of clarity. Overall, the fatigue resistance of the carbide-bearing lower bainite is smaller than that of the carbide-free lower bainite. As suggested by Long et al. [5], fatigue durability is negatively affected by the stable carbides and thick bainite ferrite plates and, on the contrary, the existence of fine bainite ferrite plates and metastable retained austenite positively affects the fatigue performance. The difference between the two tested steels is the greatest for lower lives, and tends to disappear as the strain amplitude decreases. For lives greater than 10^4, the total strain versus life curves tend to be overlapped. Regarding the transition lives, represented by $2N_T$ in Figure 7, the outcomes are also notoriously different: $2N_T$ of the carbide-bearing lower bainite is two times higher than that of the carbide-free lower bainite.
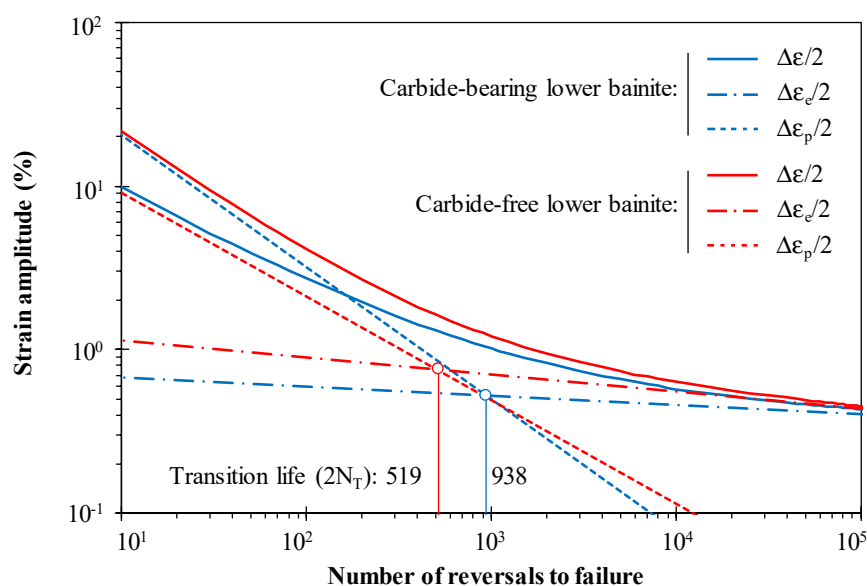
Figure 7. Strain-life relationships accounted for in terms of total strain, elastic strain, and plastic strain components for the carbide-bearing and carbide-free bainitic steels.

Table 5. Summary of the fatigue strength and fatigue ductility properties.

Material	σ_f' (MPa)	b	ε_f'	c
Carbide-bearing lower bainite	1513.44	−0.05522	0.39141	1.30301
Carbide-free lower bainite	2601.08	−0.09171	−0.63354	−0.80511

Figure 8 plots the plastic strain energy density that was evaluated from the mid-life hysteresis loops against the number of cycles to failure for the carbide-bearing and carbide-free bainitic steels. In a log-log scale, the relationship between these variables can be described by a straight line, i.e.,

$$\Delta W_p = \kappa_P (2N_f)^{\alpha_P} \tag{4}$$

where κ_P and α_P are two unknowns determined from the experimental data. The constants were calculated via the least square method and are summarised in Table 6. Not surprisingly, there is a strong correlation between these two variables. This demonstrates the adequacy of such a variable to account for the fatigue damage based on the energy dissipated [18,19].
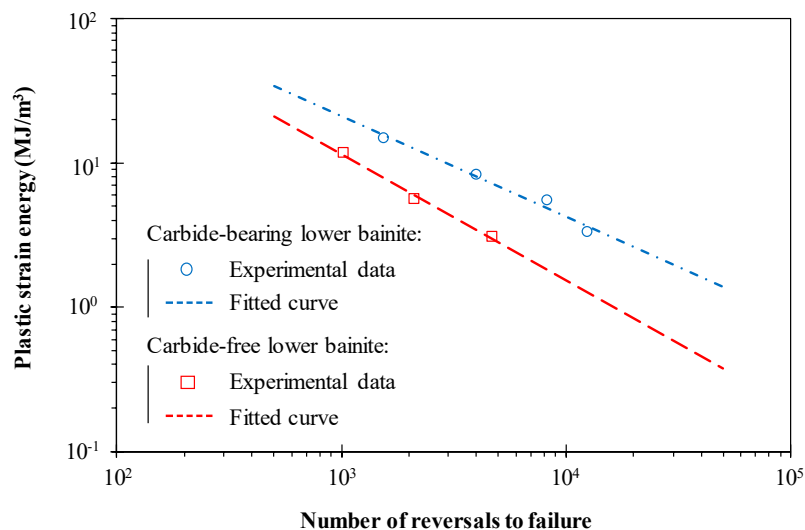
Figure 8. Plastic strain energy density versus fatigue life for the carbide-bearing and carbide-free bainitic steels.

The plastic strain energies measured in the experiments are compared in Figure 9 with those of Masing-type materials, defined as follows:

$$\Delta W_{pM} = \frac{1-n\prime}{1+n\prime}\Delta\sigma\,\Delta\varepsilon_P \tag{5}$$

where $\Delta\varepsilon_P$ is the plastic strain range, $\Delta\sigma$ is the stress range, and n' is the cyclic hardening exponent. The experimentally measured values (ΔW_p) are relatively far from those of the Masing-type materials (ΔW_{pM}) for both the carbide-bearing and carbide-free bainitic steels, and the differences increase with the strain amplitude, irrespective of the tested steel. This outcome is in line with the conclusions drawn from Figure 4.

Table 6. Summary of the energy-life properties.

Material	κ_P	α_P
Carbide-bearing lower bainite	2506.0	−0.69293
Carbide-free lower bainite	4773.1	−0.87335
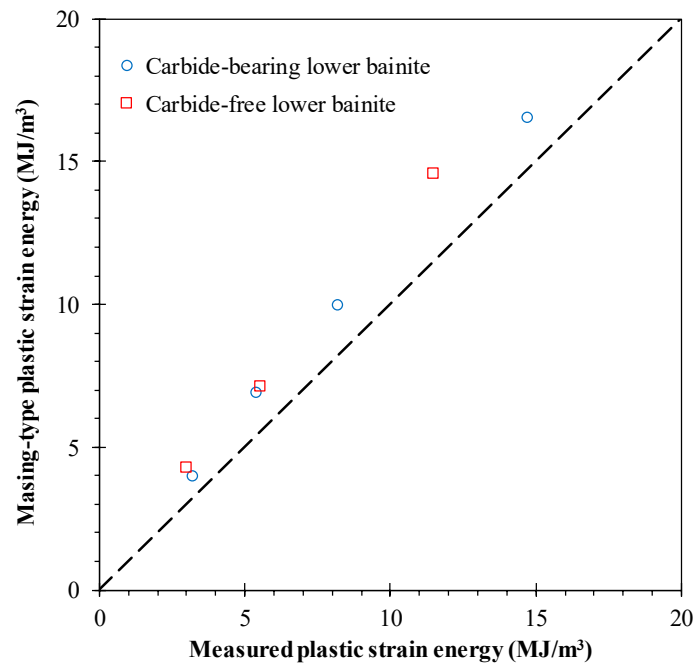
Figure 9. Comparison of the experimentally measured plastic strain energy densities (ΔW_p) and the ideal Masing-type plastic strain energy densities (ΔW_{pM}).

3.3. Analysis of Fracture Surfaces

Figure 10 shows the TEM micrographs of the carbide-free and carbide-bearing bainitic steels at strain amplitudes of 1%. The morphologies of bainite ferrite and metastable austenite, as already highlighted by Long et al. [5], are closely related to the fatigue life. Carbide-free lower-bainite steel presents higher fatigue lives under strain-controlled conditions due to the presence of fine bainitic plates which reduce its susceptibility to crack nucleation. When subjected to fatigue loading histories, metastable retained austenite gives rise to martensite, particularly in the presence of large sizes of retained austenite, as exhibited in Figure 10a. This strain-induced martensitic transformation is beneficial to increase the fatigue life in carbide-free lower-bainite steels, as it absorbs the energy required to crack propagation. In the presence of a cyclic stress state, it can lead to a tensile stress relaxation, as the tensile stress relaxation introduces compressive stresses which are likely to promote the crack closing. Regarding the carbide-bearing lower bainitic steel, it behaves differently. As documented in Figure 10b, only the occurrence of deformation is observed. As is well-known, the secondary carbide phase of the carbide-bearing lower bainitic steel is very prone to the formation of micropores which act as local stress raisers and contribute to higher rates of crack formation and, consequently, lower fatigue lives.
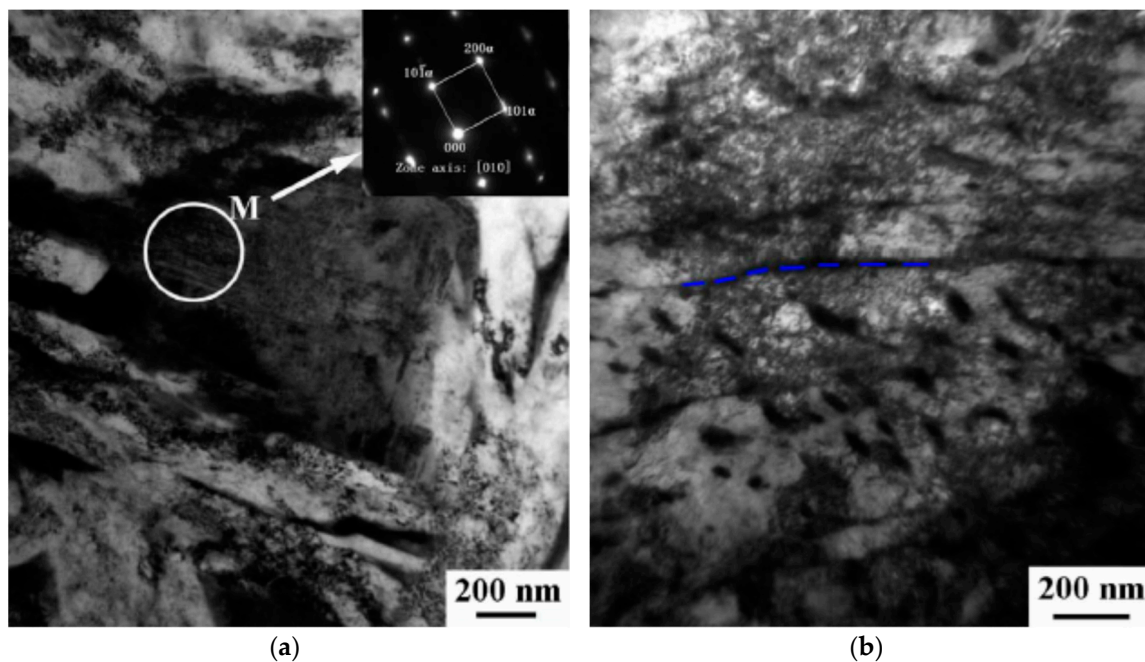
Figure 10. TEM images of low-cycle fatigue tests ($\Delta\varepsilon/2 = 1.0\%$) for the [5]: (**a**) carbide-free lower-bainite; (**b**) carbide-bearing lower-bainite. Reproduced from [5], with permission from publisher Elsevier, 2018.

4. Conclusions

This paper aimed at comparing the cyclic behaviour of carbide-bearing and carbide-free bainitic steels. In order to meet this goal, strain-controlled tests in low-cycle fatigue regime, under fully-reversed conditions at various strain amplitudes, were performed. In addition, microstructures were observed by SEM and TEM before testing, and the morphologies of the fracture surfaces were observed by TEM after total fatigue failure. The following conclusions can be drawn:

- The microstructure of the carbide-free lower bainite is formed by bainitic ferrite and retained austenite of varying size, while the microstructure of the carbide-bearing lower bainite is formed by bainitic ferrite and carbides that are distributed within the bainitic ferrite or between the bainitic ferrite;
- The cyclic stress response of the tested steels comprises three different stages: an initial cyclic hardening behaviour with a strong effect in the early cycles, followed by a smoother decrease of the stress amplitude; a second stage, close to a saturated response, with tenuous cyclic stress variations; and a final stage of a marked reduction of stress amplitude until fatigue failure occurs;
- The maximum stress amplitudes, under strain-controlled conditions, are observed in the early cycles of the tests for life ratios lower than 1%, irrespective of the strain amplitude. Regarding the ratios of the initial stress amplitude to the maximum stress amplitude, it can be noted that the responses of both steels are similar, with ratios close to 1—or more precisely, 0.93 and 0.97 for the carbide-bearing lower bainite and carbide-free lower bainite, respectively;
- The shapes of the mdi-life hysteresis loops at similar strain amplitudes are quite different. The area—i.e., the plastic strain energy density—is higher for the carbide-bearing lower bainite. However, in both cases, we are in the presence of non-Masing type materials which are associated with the changes in the linear region of the stable circuits;
- Based on the differences between the monotonic curve and the cyclic stress-strain curve that were evaluated from the mid-life circuits, it was possible to identify two antagonistic responses: the carbide-bearing lower bainite exhibited a strain-softening behaviour, while the carbide-free

lower bainite was characterised by a strain-hardening behaviour. The degree of softening was in the range of 3–15%, and the degree of hardening varied within the range of 3–8%;

- The fatigue resistance of the carbide-bearing lower bainite is lower than that of the fatigue resistance of the carbide-free lower bainite. At low strain amplitudes, the differences are more relevant. Nevertheless, for lives greater than 10^4 reversals, the fatigue responses tend to be similar. With regard to the transition lives, the main outcomes are markedly different: the transition life of the carbide-bearing lower bainite is almost twice the value of the carbide-free lower bainite;

- Fracture surface morphologies of the carbide-free lower bainite exhibited fine bainitic plates which are associated with a reduced susceptibility to crack nucleation, which contributes to higher fatigue resistance, which is verified in the experiments.

References

1. Caballero, F.G.; Santofimia, M.J.; García-Mateo, C.; Chao, J.; Andrés, C.G. Theoretical design and advanced microstructure in super high strength steels. *Mater. Des.* **2009**, *30*, 2077–2083. [CrossRef]

2. Zhang, F.C.; Yang, Z.N.; Kang, J. Research progress of bainitic steel used for railway crossing. *J. Yanshan Univ.* **2013**, *37*, 1–7.

3. Aglan, H.A.; Liu, Z.Y.; Hassan, M.F.; Fateh, M. Mechanical and fracture behavior of bainitic rail steel. *J. Mater. Process. Technol.* **2004**, *151*, 268–274. [CrossRef]

4. Georgiyev, M.N.; YuKaletin, A.; Siminov, Y.N.; Schastlivtsev, V.M. Influence of stability of retained austenite on crack resistance of engineering steel. *Phys. Met. Metall.* **1999**, *69*, 110–118.

5. Long, X.; Zhang, F.; Yang, Z.; Lv, B. Study on microstructures and properties of carbide-free and carbide-bearing bainitic steels. *Mater. Sci. Eng. A* **2018**, *715*, 10–16. [CrossRef]

6. Zhang, F.C.; Long, X.Y.; Kang, J.; Cao, D.; Lv, B. Cyclic deformation behaviors of a high strength carbide-free bainitic steel. *Mater. Des.* **2016**, *94*, 1–8. [CrossRef]

7. Long, X.Y.; Zhang, F.C.; Zhang, C.Y. Effect of Mn content on low-cycle fatigue behaviors of low-carbon bainitic steel. *Mater. Sci. Eng. A* **2017**, *697*, 111–118. [CrossRef]

8. Golos, K.M.; Debski, D.K.; Debski, M.A. A stress-based fatigue criterion to assess high-cycle fatigue under in-phase multiaxial loading conditions. *Theor. Appl. Fract. Mech.* **2014**, *73*, 3–8. [CrossRef]

9. Lu, C.; Melendez, J.; Martínez-Esnaola, J.M. A universally applicable multiaxial fatigue criterion in 2D cyclic loading. *Int. J. Fatigue* **2017**, *110*, 95–104. [CrossRef]

10. Branco, R.; Costa, J.D.; Berto, F.; Antunes, F.V. Effect of loading orientation on fatigue behaviour in severely notched round bars under non-zero mean stress bending-torsion. *Theor. Appl. Fract. Mech.* **2017**, *92*, 185–197. [CrossRef]

11. Wu, S.C.; Zhang, S.Q.; Xu, Z.W.; Kang, G.Z.; Cai, L.X. Cyclic plastic strain based damage tolerance for railway axles in China. *Int. J. Fatigue* **2016**, *93*, 64–70. [CrossRef]

12. Madrigal, C.; Navarro, A.; Chaves, V. Numerical implementation of a multiaxial cyclic plasticity model for the local strain method in low cycle fatigue. *Theor. Appl. Fract. Mech.* **2015**, *80*, 111–119. [CrossRef]

13. Branco, R.; Prates, P.; Costa, J.D.; Berto, F.; Kotousov, A. New methodology of fatigue life evaluation for multiaxially loaded notched components based on two uniaxial strain-controlled tests. *Int. J. Fatigue* **2018**, *111*, 308–320. [CrossRef]

14. Firat, M. A numerical analysis of combined bending-torsion fatigue of SAE notched shaft. *Finite Elem. Anal. Des.* **2012**, *54*, 16–27. [CrossRef]

15. Branco, R.; Costa, J.D.; Antunes, F.V.; Perdigão, S. Monotonic and cyclic behaviour of DIN 34CrNiMo6 martensitic steel. *Metals* **2016**, *6*, 98. [CrossRef]

16. Branco, R.; Costa, J.D.; Berto, F.; Razavi, S.M.J.; Ferreira, J.A.M.; Capela, C.; Santos, L.; Antunes, F.V. Low-cycle fatigue behaviour of AISI 18Ni300 maraging steel produced by selective laser melting. *Metals* **2018**, *8*, 32. [CrossRef]

17. Morrow, J. Cyclic plastic strain energy and fatigue of metals. In *International Friction, Damping and Cyclic Plasticity*; ASTM STP 378; American Society for Testing and Materials: Philadelphia, PA, USA, 1965; pp. 45–87.

18. Song, W.; Liu, X.; Berto, F.; Razavi, S. Low-cycle fatigue behavior of 10CrNi3MoV high strength steel and its undermatched welds. *Materials* **2018**, *11*, 661. [CrossRef] [PubMed]

19. Branco, R.; Costa, J.D.; Berto, F.; Antunes, F.V. Fatigue life assessment of notched round bars under multiaxial loading based on the total strain energy density approach. *Theor. Appl. Fract. Mech.* **2018**, in press. [CrossRef]